BEFIB2012 – Fibre reinforced concrete
Joaquim Barros et al. (Eds)

INTERFACIAL BOND BEHAVIOUR OF GFRP BAR IN SELF-COMPACTING FIBER REINFORCED CONCRETE

H. Mazaheripour*, J. Barros*, F. Soltanzadeh* and D. Gonçalves†

* ISISE, Dep. Civil Eng., School Eng., University of Minho
Campus de Azurém 4800-058 Guimarães, Portugal
e-mail: hmp@civil.uminho.pt

† Civitest company,
4760-042 Vila Nova de Famalicão, Portugal
e-mail: delfinagoncalves@civitest.com, web page: www.civitest.pt

Keywords: Bond, interface, GFRP, self-compacting concrete, FRC.

Summary: *In an ongoing research project, discrete steel fibers are being used in a self-compacting concrete (SFRSCC) to replace completely steel stirrups for pre-fabricated beams reinforced longitudinally with pre-stressed glass fiber reinforced polymer (GFRP) and steel bars. To take the advantages of the non-corrodible character and high tensile strength of GFRP bars, the minimum SFRSCC cover needs to be determined in order to assure the adequate bond performance between these bars and the surrounding SFRSCC. Since bond of the longitudinal bars has a relevant impact on the cracking behavior of RC elements (crack opening and crack spacing), an extensive experimental program composed of pullout bending tests was carried out where the influence of the following parameters was assessed in terms of bond behavior: GFRP bar diameter, surface characteristics of the GFRP bars, bond length, SFRSCC cover thickness. The local bond law was derived from inverse analysis and it was used to define the slip mode of the constitutive law adopted for interface finite elements. These interface finite elements were used to assess the crack opening and crack spacing on SFRSCC beams flexurally reinforced with GFRP bars. This paper resumes the experimental program, describes the strategy to derive the local bond law and presents and discusses the numerical simulations.*

1 INTRODUCTION

It was more than two decades that GFRP was introduced in the construction industry as a non-corrodible material for an alternative to the steel bars, especially in aggressive environments. Due to the relative low Young's modulus, and the linear behavior up to failure, the deflection limits imposed by serviceability design limit states and ductility requirements for reinforced concrete structures have imposed restrictions on the use of these composite materials. A great deal of effort has been made up to now for improving ductility index and serviceability limit (crack width and crack spacing) of FRP reinforced concrete structures. In the literature three strategies are being pointed out in this context: using hybrid FRP materials [1]; using hybrid steel and FRP [2-4]; and finally using concrete of enhanced properties [3-5].

This study is part of a research project with the main objective of developing a reinforcing system composed of pre-stressed GFRP and steel bars for the flexural reinforcement of fiber reinforced concrete (FRC) pre-fabricated beams, where discrete fibers are used to eliminate the use of steel stirrups. The use of fibers has also the purpose of improving the bond behavior between longitudinal bars and surrounding concrete, and enhancing the fire resistance of these structural elements. The steel bars would be mounted with lower internal arm in order to have larger FRC cover for higher protection against corrosion, while GFRP bars would be placed near the tensile surface in order to

have a higher internal arm and, therefore, mobilizing more efficiently their reinforcement capabilities.

In general, the available bibliography reports that the bond strength of FRP bars is lower than of steel bars [6,7]. Furthermore, since there is the aim of increasing the internal arm of the FRP bars, the minimum FRC cover that assures the necessary bond requisites should be determined. Despite many experimental tests have been carried out for the evaluation of FRC-concrete bond behavior [6-17], it is still lack of consensus on the methodology to assess the data that can be used to define reliable local bond equations. The curve fitting method is still being used to estimate local bond-slip law parameters [6,12-14,17,18]. The common test setup in the literature is the direct pullout test [19]. However, some studies used pullout bending test setup and they reported that the beam test may provide more real bond behavior due to the elimination of confinement that is observed in case of direct pullout test [6].

In this study an experimental program composed of pullout bending tests (the test setup is similar to that recommended by RILEM [19]) was carried out to obtain the bond-slip constitutive law for modeling the interface between GFRP bars and steel fiber reinforced concrete (SFRSCC). The influence of bond length, bar diameter and SFRSCC cover thickness in the bond behavior was investigated. The derived bond constitutive law was used for modeling the sliding component of interface finite elements, and the influence of the FRC-SFRSCC bond performance on the crack width of SFRSCC beams flexurally reinforced with GFRP and steel bars was assessed by performing material nonlinear analysis with a FEM-based computer program.

2 EXPERIMENTAL PROGRAM

The experimental program in this study is composed of two steps. First, a self-compacting concrete reinforced with 60 kg/m^3 of hooked ends steel fibers was developed and its relevant properties were determined from experimental tests. In the second step pullout bending tests were executed to derive data for the development of constitutive laws capable of modeling the GFRP-SFRSCC bond behavior.

2.1 Materials

2.1.1 Steel fiber reinforced self compacting concrete

The mix is composed of ordinary Portland cement CEM I 42.5 R (412 kg/m^3), limestone filler (353 kg/m^3), fine and coarse river sand (179 and 655 kg/m^3, respectively), crushed granite gravel aggregate (588 kg/m^3) with maximum size of 12 mm, 1.9% of cement content of super-plasticizer, the water/cement ratio of 0.39, and 60 kg/m^3 hooked ends steel fibers with a length (L_f) and a diameter (d_f) of 33mm and 0.55 mm, respectively (L_f/d_f=60). For the batches in the specimens' preparation, slump-flow tests were executed, and slump flow values in the interval 680 to 720 mm were obtained, without occurrence of segregation. Cube and cylinder specimens were casted to assess the SFRSCC compressive strength. Cylinders were also used for measuring the SFRSCC Young's modulus. The obtained results included in Table 1 reveal that the mean value of the obtained Young's modulus is about 19% smaller than the value suggested by fib [20] for conventional concrete. This was expectable since a higher amount of binder is used in SFRSCC [21, 22].

Table 1: Compressive strength and Young's modulus of SFRSCC

	f_{cm}[1] *MPa*	f_{ck}[2] *MPa*	*Concrete Grade* [2]	*Young's modulus* *N/mm^2*	*N/mm^2*
SFRSCC (CoV)	63.68 (5.51%)	55.68	C50	30360 [3] (15.48%)	35959 [4]

[1] Mean value from 9 cube and 8 cylinder specimens; [2] Based on fib code [20] ; [3] From 4 cylinder specimens; [4] Based on the equation provided by fib code, assuming limestone aggregates

For the characterization of the post-cracking behavior of the SFRSCC, three point notched beam bending tests were carried out according to the final recommendation of RILEM [23]. The results in

terms of force versus both the crack mouth opening displacement (CMOD) and mid span deflection (δ) are plotted in figure 2. The δ-CMOD relationship is represented in figure 3b, as well as the equation recommended by RILEM, where it can be concluded that this equation provides a good correlation between these entities. Table 2 includes the residual tensile strength parameters for CMOD equal to 0.5 1.5, 2.5 and 3.5 mm (f_{R1}, f_{R2}, f_{R3}, f_{R4}), the stress at crack initiation (also designated as limit of proportionality, LOP) for the 5 tested SFRSCC. The average Force-CMOD curve is plotted in figure 3a and the mean valuemean values for the f_{Ri} are also indicated.

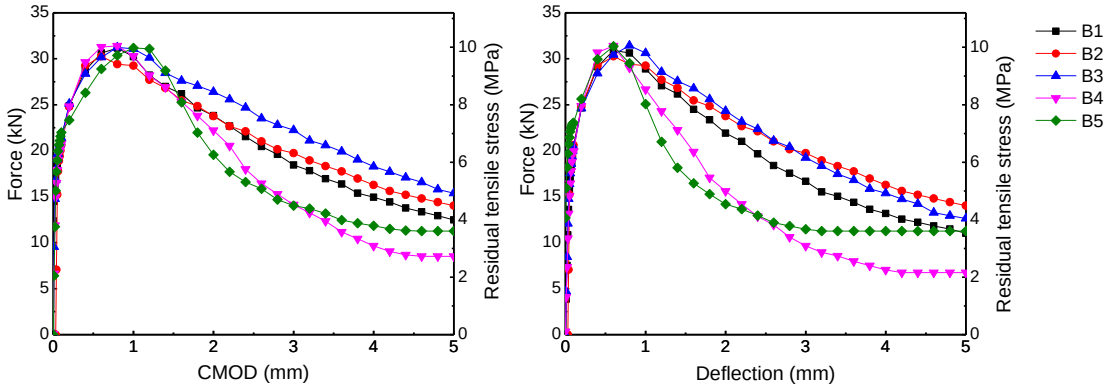

Figure 2: Force/residual stress versus CMOD and force/residual stress versus δ from the experimental tests

Table 2: Residual flexural tensile strength parameters of SFRSCC

Specimen Identification	Notched beam geometry			Residual tensile strength parameters						LOP *
				$CMOD_1$=0.5	$CMOD_2$=1.5	$CMOD_3$=2.5	$CMOD_4$=3.5			
	l	b	h_{sp}	f_{R1}	f_{R2}	f_{R3}	f_{R4}	$\frac{f_{R3}}{f_{R1}}$	F_L	$f^f_{ct,L}$
	mm	mm	mm	MPa	MPa	MPa	MPa		kN	MPa
NB1	500	152	125.2	9.09	8.52	6.80	5.35	0.75	18.47	5.83
NB2	500	151	125.4	9.24	8.47	6.98	5.79	0.75	15.23	4.81
NB3	500	151	125.5	8.97	9.00	7.81	6.51	0.87	19.06	6.03
NB4	500	138	116.3	11.90	11.81	7.23	4.96	0.61	17.90	7.19
NB5	500	150	112.2	10.45	11.40	6.59	5.23	0.63	18.96	7.53
Average: (CoV):				**9.93 (12.6%)**	**9.25 (14.21%)**	**6.97 (6.61%)**	**5.54 (10.89%)**	**0.73**	**17.92 (8.79%)**	**6.28 (17.49%)**

* Limit of proportionality;

To determine the tensile stress-strain (σ-ε) and the stress-crack opening (σ-w) relationships that will be used later on the FEM-based simulations of SFRSCC hybrid reinforced beams, two methods are followed in this paper based on inverse analysis. The σ-ε was obtained by using a cross section layer model capable of determining the moment-curvature relationship of a beam's cross section. In this approach, which methodology is exposed elsewhere [24], the σ-ε tensile diagram is obtained from inverse analysis by fitting with the minimum error the average force-deflection curve recorded in the experimental tests. In its turn, the σ-w is obtained by performing finite element analysis, where interface finite elements are localized along the symmetry axis of the notched beam (Figure 4). In this approach the σ-w trilinear diagram that defines the crack opening mode of the constitutive law of the interface finite elements is derived from inverse analysis by matching with the minimum error the average force-deflection curve of the experimental results [25]. The obtained σ-w and σ-ε diagrams are represented in Figure 5a and 5b, respectively. In these figures are also indicated the values that define these diagrams, as well as the mode I fracture energy, G_f, derived from the area under the σ-w diagram. Two trilinear diagrams have been presented for σ-w in Figure 5a Trend 1 was obtained by

minimizing an error parameter that is the ratio between the area limited by the experimental and the numerical curves and the area underneath the experimental curve, but limiting this analysis up to a deflection of 5.0 mm. In trend 2 the minimization of the error parameter was performed up to 1.0 mm. Taking these two trends for modeling the post-cracking behavior of SFRSCC, the numerically obtained F-δ relationships are compared to the experimental curve in Figure 5c. It is evident that trend 2 matches better the experimental F-δ up to δ=1.0 mm (error of 0.10% for trend 2 and 2.79% for trend 1), while trend 1 fits closer up to δ=5.0 mm (error of 0.60% for trend 1 and 16.78% for trend 2). Hence, trend 1 and its corresponding G_f (7.55 *N/mm*) may be applicable for the simulations of SFRSCC for ultimate limit state conditions, while the tri-linear stress-crack opening diagram shown by trend 2 can be adopted for the simulations corresponding to serviceability limit state conditions. According to fib Model Code [20] the post-cracking tensile strain can be obtained from the crack with by using the concept of a characteristic length, that for the notched beam is the depth of the notched section (h_{sp}=125mm). Applying the characteristic length to the σ-w of Figure 5a (trend 1), the dotted σ-ε diagram represented in Figure 5b is obtained, which matches quite well the σ-ε diagram derived from inverse analysis by using the moment-curvature approach [22]. This indicates that the tensile σ-ε diagram can be obtained by applying the concept of characteristic length proposed by fib Model Code to the σ-w diagram derived from inverse analysis with a FEM-based approach.

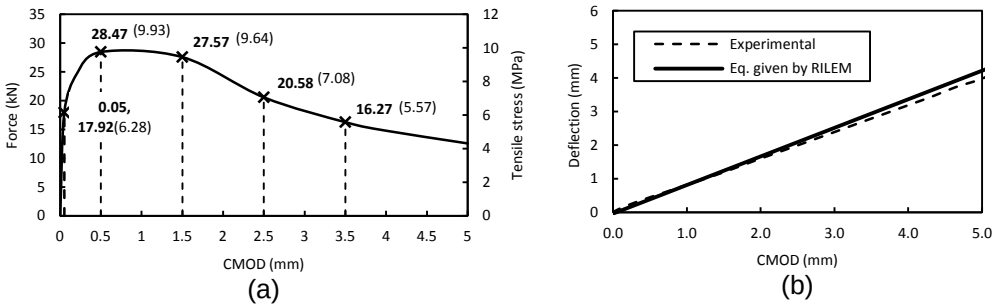

Figure 3: The average Force/Stress-CMOD (a) The δ-CMOD relationship (b)

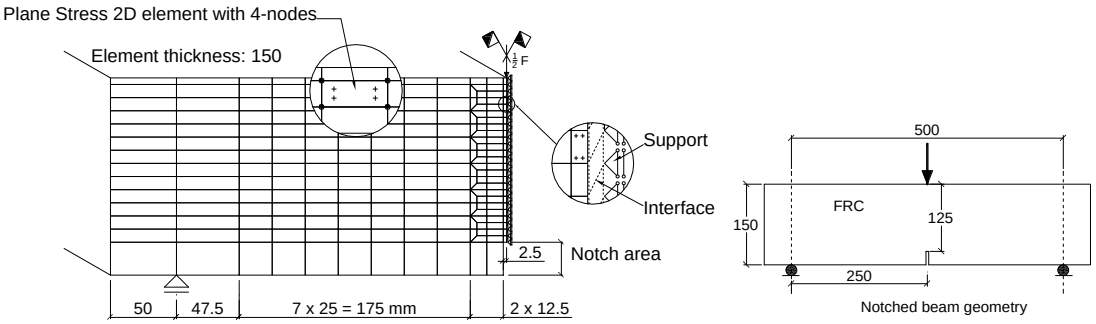

Figure 4: FEM-based inverse analysis approach to derive the stress-crack width relationship (dimensions in mm)

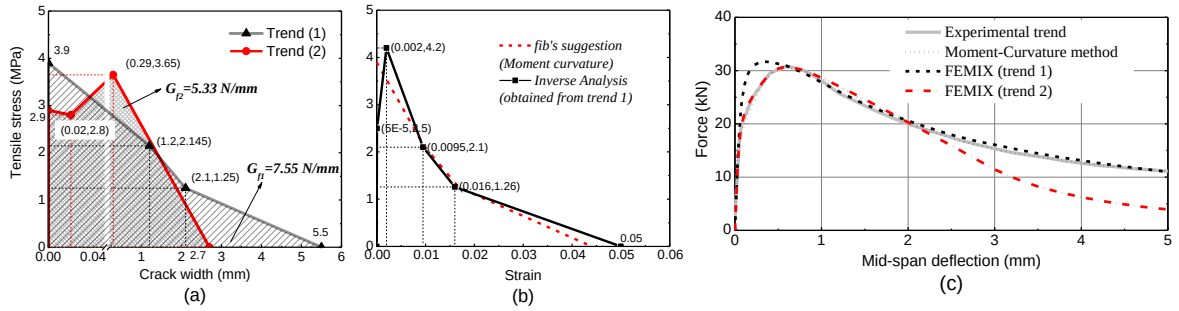

Figure 5: Tensile stress-crack width (a) and tensile stress-strain diagrams (b) derived from inverse analysis (c)

2.1.2 Glass fiber reinforced polymer (GFRP)

Table 4 includes the properties of GFRP bars of 8 and 12 mm diameter (ϕ) provided by the supplier. The surface treatment of the bars is almost the same apart the rib height that is dependent of the bar diameter. According to the supplier the modulus of elasticity (E_f) of both bars is 60 *GPa*, but the tests carried out have provided an mean value of 67 and 71 *GPa* for ϕ8 and ϕ12 bars, respectively. These bars have linear and elastic behavior up to failure.

Table 4: Mechanical properties of GFRP bar

Bar diameter *mm*	Surface treatment		Modulus of Elasticity [1]	Tensile strength	Density	Content of glass	Modulus of Elasticity [2]
	Rib spacing *mm*	Rib height *mm*	*N/mm²*	*MPa*	*gr/cm³*	%	*N/mm²*
8	8.5	0.35-0.5	60,000	~1,500	2.23	~75	71,000
12	8.5	0.5-0.75	60,000	~1,350	2.23	~75	67,000

[1] Reported by the manufacturer
[2] Mean value of 5 specimens

2.2 Pullout bending tests

A total of 24 pullout bending tests were carried out according to the test setup recommendations of RILEM in 1982 for steel bars [19]. The specimen includes two SFRSCC blocks that are connected with a steel hinge at top (compression zone) and a GFRP bar is mounted as a flexural reinforcement at bottom (Figure 6). Two types of bar diameter, two SFRSCC cover thicknesses (15 and 30 mm) and three different bond lengths (5ϕ, 10ϕ and 20ϕ) were considered the parameters whose influence on the bond behavior is intended to be investigated. The slip at loaded and free ends (s_l, s_f, respectively) were measured by using two displacement transducers (LVDT1 and LVDT2, respectively, Figure 6). The force applied to the bar was determined from the strain recorded in a strain gauge installed at the middle of the bar and taking the E_f and the cross sectional area of the bar, A_f. The tests were carried out by using a closed-loop servo hydraulic control system with capacity of 200kN. Two slipping test control regimes of different slip rate were adopted: 3 μm/sec until 5 mm slip; 5 μm/sec up to the end of the test.

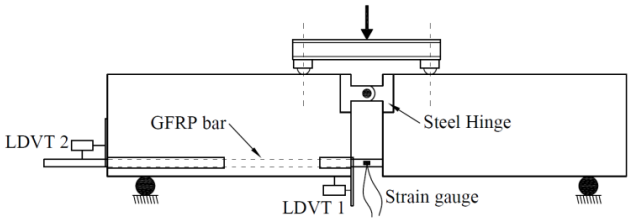

Figure 6: Pullout bending test setup

The pullout failure was observed for all specimens with the exception of one specimen reinforced with a 8 mm bar diameter and with 20ϕ bond length. For specimens with 15 mm SFRSCC cover and 12 mm bar diameter a splitting crack was observed along the bond length in the alignment of the bar, at the bottom surface of the SFRSCC block. The occurrence of this crack can justify the lower maximum bond strength registered in the specimens with the minimum SFRSCC cover thickness. However, the crack did not appear for 5ϕ bond length.

The relationships between the pullout force and the slip at loaded and free ends are represented in Figures 7 to 10 for all the tested specimens. The bond strength of both bar diameters was almost the same, but it has decreased with the increase of the bond length. However, it has been reported in the literature that the bond strength has a tendency to decrease with the increase of the bar diameter [7,13].

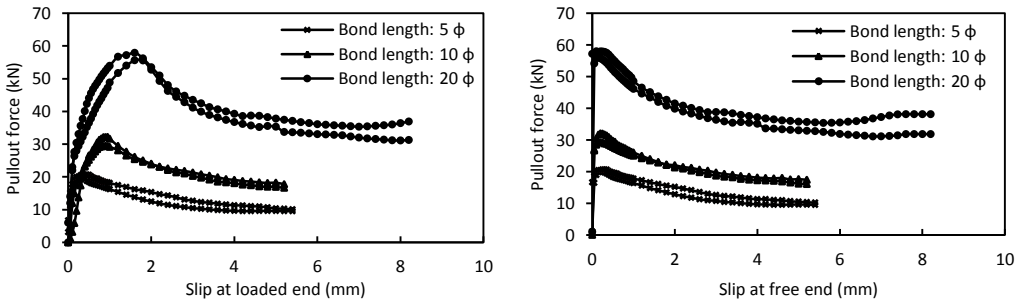

Figure 7: Pullout force versus slip for 8 mm bar diameter with 15 mm SFRSCC cover

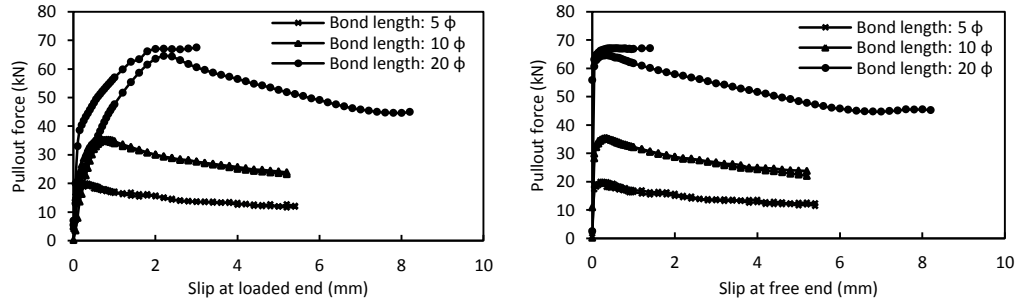

Figure 8: Pullout force versus slip for 8 mm bar diameter with 30 mm SFRSCC cover

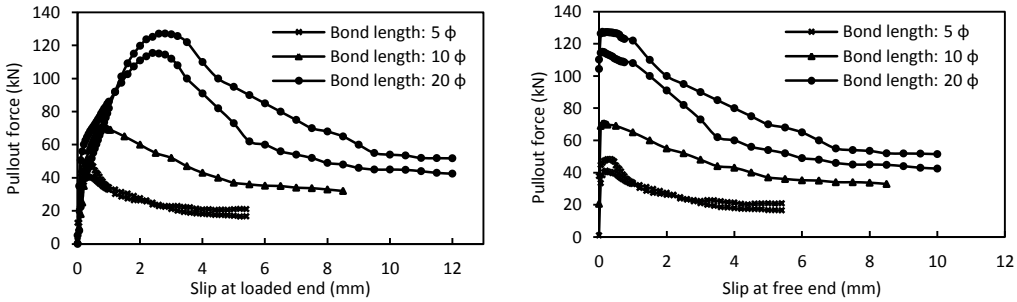

Figure 9: Pullout force versus slip for 12 mm bar diameter with 15 SFRSCC cover

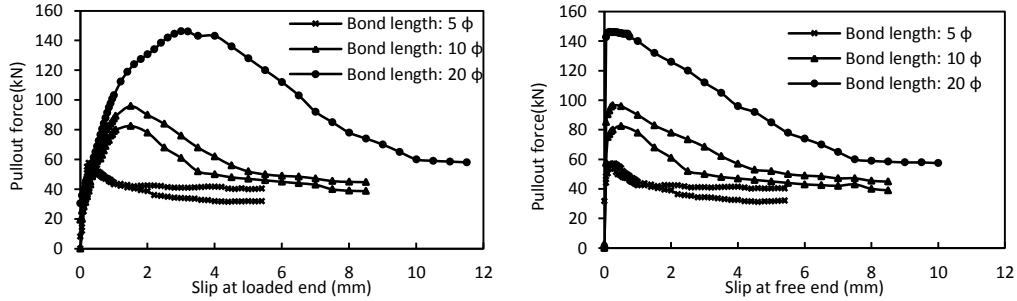

Figure 10: Pullout force versus slip for 12 mm bar diameter with 30 SFRSCC cover

3 NUMERICAL STUDY

In this chapter the bond tests are simulated numerically by using version 4.0 of FEMIX computer program (Azevedo et al., 2003). This program is also used to assess the influence of modeling the bond conditions of GFRP bars-surrounding SFRSCC on the maximum crack opening of a SFRSCC beam reinforced according to the hybrid concept proposed in the present work.

3.1. Simulation of the pullout bending tests

To simulate the bond between GFRP bar and concrete, an interface finite element with a non-linear constitutive law is used. Figure 11 shows the specific model for a specimen with 8 mm bar diameter, 15 mm concrete cover and 5ϕ bond length. The connection between interface element, GFRP bar and SFRSCC is also illustrated. The non-linear behavior of interface element is defined according to the following equation:

$$\tau(s)=\begin{cases}\left(\dfrac{\tau_0}{s_0}\right)s & s<s_0\\ \left(\dfrac{s}{s_m}\right)^{\alpha}\tau_m & s_0\le s<s_m\\ \left(\dfrac{s}{s_m}\right)^{\beta}\tau_m & s\ge s_m\end{cases} \quad (1)$$

where τ_0 and s_0 are the bond stress and the corresponding slip at the end of the first linear branch, τ_m and s_m are the bond strength and the corresponding slip respectively, and α and β are parameters that define the shape of the pre-peak and post-peak branches.

The SFRSCC pullout-beam was discretized by Lagrangian 4-node plane stress finite elements of linear and elastic behavior, with E_c=29 GPa and ν_c=0.2, and an integration scheme of 2×2 was adopted. The GFRP bar was simulated by 2D truss elements of 2 nodes, and a linear and elastic behavior was assumed, with an integration rule of 2 points. Linear 4-node interface elements with an integration scheme of 2 points was applied with a constant normal stiffness of 0.1 MN/mm and a tangential stiffness provided by Equation (1) where the parameters were determined from inverse analysis, by fitting the pullout force versus loaded end slip with the minimum error (Figures 12, 13 and 14). Since a 2D simulation was performed in this study, the interface was applied with a constant thickness equals to the perimeter of the bar calculated by means of πd_b (d_b: bar diameter).

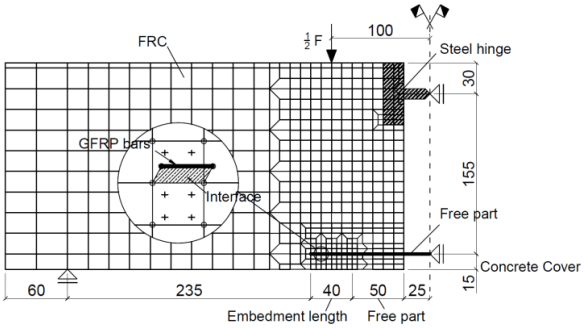

Figure 11: Finite element model to simulate pullout bending tests (example for 8 mm bar diameter with 5ϕ bond length and 15 mm SFRSCC cover (dimensions in mm)

The values that define the obtained bond slip law are included in Table 5, where it can be concluded that the maximum bond strength (τ_m) is almost same for both bar diameters. Furthermore, by increasing in bond length the maximum bond strength has decreased.

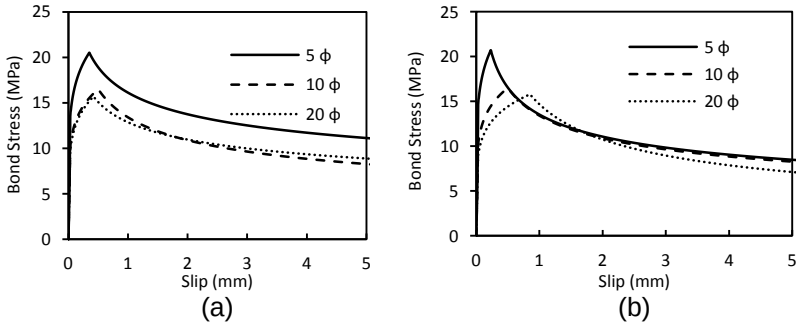

Figure 12: Bond-slip relationships determined from numerical modeling by inverse analysis for the specimens reinforced with GFRP bar diameter of: (a) 8 (b) 12 mm

Table 5: Values that define the bond-slip law determined from numerical simulation of the pullout bending tests

Specimen configuration			Adopted bond slip law					
Bond length mm	Concrete cover mm	Bar diameter mm	τ_0 MPa	s_0 mm	τ_m MPa	s_m mm	α	β
5ϕ	15	8	10	0.03	20.5	0.35	0.17	0.23
10ϕ	15	8	10	0.03	16.5	0.50	0.17	0.30
20ϕ	15	8	10	0.03	15.7	0.42	0.18	0.23

5ϕ	15	12	10	0.03	20.7	0.23	0.17	0.29
10ϕ	15	12	10	0.03	16.5	0.50	0.17	0.30
20ϕ	15	12	10	0.03	15.8	0.85	0.17	0.45

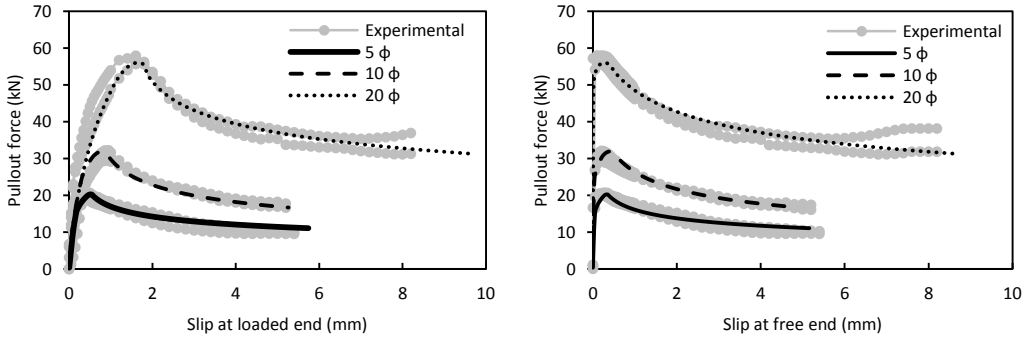

Figure 13: Comparison between numerical and experimental results in context of pullout force-slip; ϕ8 bar diameter

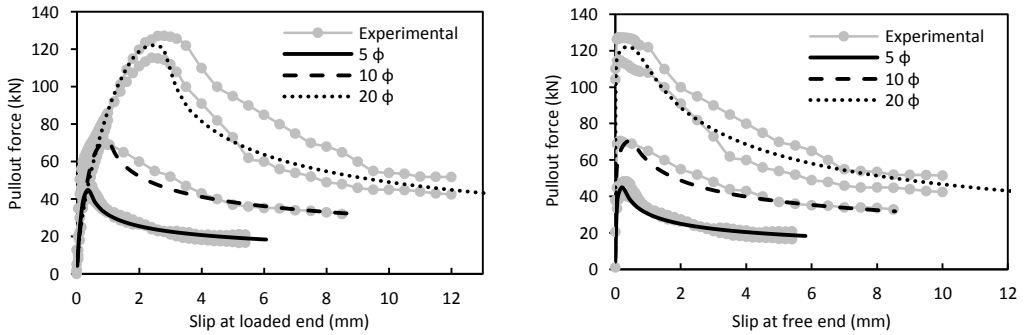

Figure 14: Comparison between numerical and experimental results in context of pullout force-slip; ϕ12 bar diameter

3.2. Application

To assess the influence of the GFRP-SFRSCC bond conditions on the maximum crack width of SFRSCC beams flexurally reinforced with GFRP and steel bars, a material nonlinear analysis with the FEMIX computer program was carried out with the beam represented in Figure 15. The SFRSCC beam was discretized by Lagrangian 4-node plane stress finite elements with 2×2 Gauss Legendre integration scheme. The smeared crack model described by Barros et al. [26] was used to simulate the crack initiation and propagation in SFRSCC, where the diagram of Figure 5b, obtained from inverse analysis, was selected to simulate the crack normal stress versus crack normal strain, with the mode I fracture energy indicated in Figure 5a, and adopting for the crack band width a value equal to the square root of the area of the integration point (in order to assure mesh objectivity [27]). The total shear approach described in [26] was used to simulate the crack shear behavior, and a maximum number of 2 cracks per integration point was allowed, with a threshold angle of 30 degrees and the principal tensile stress higher than the tensile strength for the criteria to open a new crack. The GFRP bar (ϕ=12mm) was modeled like in the bond tests, and the steel bar (ϕ=12mm) was simulated by embedded cable elements of 2 nodes with 2 Gauss-Legendre integration scheme, assuming an elasto-plastic behavior with a yield stress of 350 MPa and the elasticity modulus of 200 GPa. Two

simulations were carried out assuming for both that steel bar is perfectly bonded to surrounding concrete, but the GFRP-SFRSCC conditions are different in these two simulations: i) assuming the bond-slip equation (1) with the parameters indicated in Table 5 for the GFRP of 12 mm diameter with a bond length of 20ϕ and a SFRSCC cover of 15 mm; ii) perfect bond.

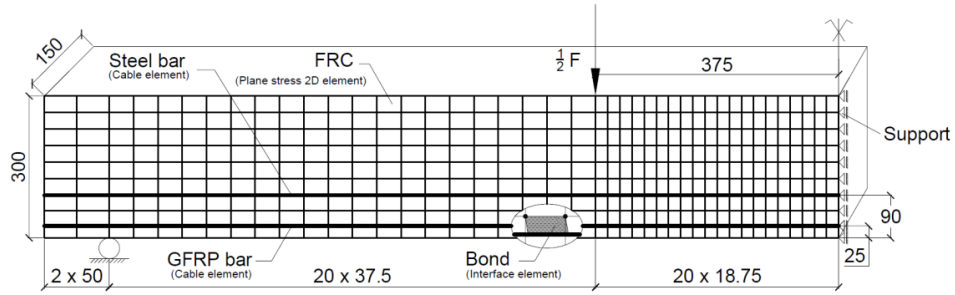

Figure 15: Finite element model for simple supported beam reinforced with GFRP and steel bars

Figure 16 illustrates two deformed meshes at the last load combination for both simulations; one with assuming perfect bond of GFRP-SFRSCC (right side figure) and the second with allowing slip between GFRP bar and SFRSCC (left side figure). As shown, the maximum crack width increases significantly when GFRP-SFRSCC sliding is simulated.

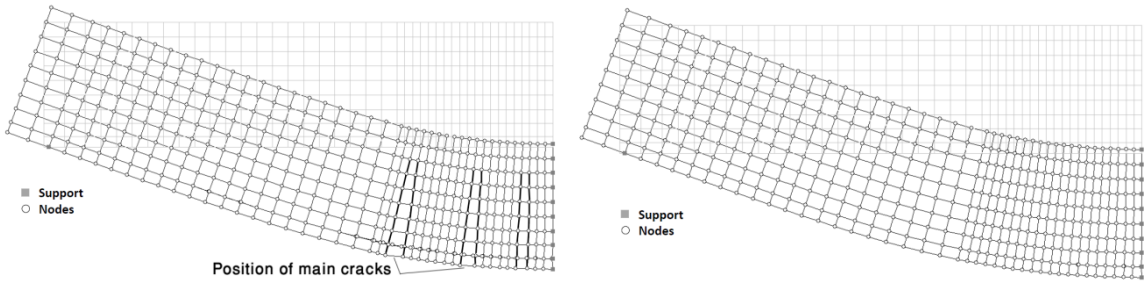

Figure 16: Deformed mesh at the last load combination: modeling the sliding between GFRP bars and surrounding SFRSCC (left figure); assuming perfect bond (right figure)

The applied load versus mid-span deflection of the beam for two GFRP-SFRSCC bond conditions and two percentages of GFRP bars is plotted in figure 17a, where n_f is the number of GFRP bars. This figure shows that up to a deflection of about the one corresponding to the service limit state (≅10 mm) the bond conditions do not have relevant effect, but above this deflection level the load carrying capacity is higher when perfect bond is assumed, and the favorable effect of the bond conditions is as pronounced as higher is the number of GFRP bars applied. Figure 17b represents the relationship between the maximum tensile stress in the GFRP bar and the maximum crack width at the level of the GFRP bar for the two bond conditions and for two distinct percentages of GFRP bars. The crack width is obtained by multiplying the crack normal strain in the direction of the beam's axis by the crack band width. It is visible that for a certain maximum tensile stress in the GFRP bars the maximum crack width occurred when sliding is allowed. If a maximum crack width of 0.3 mm is imposed this limit is attained for lower maximum tensile stress in the GFRP in case of assuming sliding between GFRP bars and surrounding SFRSCC. If two GFRP bars of perfect bond are assumed, this limit is never attained.

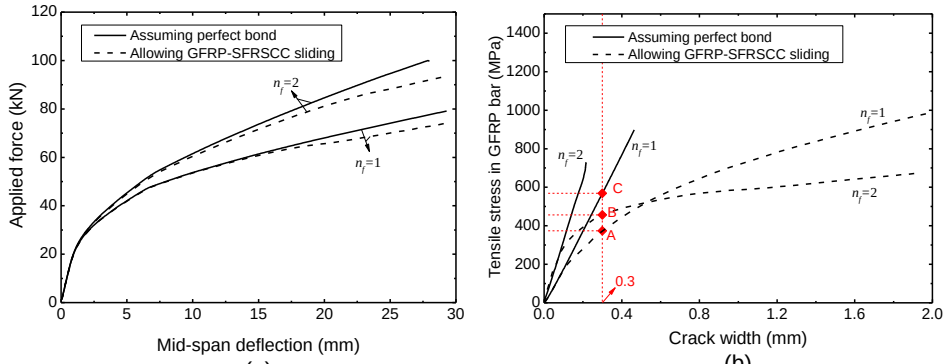

Figure 17: (a) Applied load versus mid-span deflection (b) Tensile stress in GFRP bar versus crack width

4 CONCLUSIONS

According to what investigated in this paper, the following conclusion can be drawn:

- A concrete mix design composed of 60kg/m^3 steel fibers with using self-compacting method was developed in this study and a high-performance steel fiber reinforced concrete was attained. Due to the relatively high amount of binder in this type of mix design, the value of modulus of elasticity is lower than the value given by fib [20] based on the compressive strength of concrete (f_{cm}).
- Based on inverse analysis, two methods were followed in this study to determine the crack-opening and tensile stress-strain relationship of SFRSCC in bending. The fitting accuracy of both methods of inverse analysis was acceptable and the mode I fracture energy (G_f) was approximated well from the area under tensile stress versus crack opening diagram.
- 15 mm concrete cover thickness is not proper for GFRP of 12mm bar diameter. A splitting crack appeared in the specimens for that case. In case of GFRP bar, it is predicted that the splitting concrete cover would be occurred when SFRSCC cover less than 2d is used. However, this phenomenon may be improved when a higher amount of steel fiber for concrete is used; more investigations are suggested in that case.
- The average maximum bond strength in GFRP bar decreases when the bond length of that bar increases.
-
- The non-linear interface finite element used in this study shows an acceptable capability to predict the interfacial bond behavior between GFRP bar and self-compacting fiber reinforced concrete in context of bending behavior.
- Based on the numerical results, the non-linear interface finite element also shows the impact of bond conditions of GFRP bar on the serviceability limit states of beam structure. For purposed beam, up to a deflection of about 10 mm, the bond-slip relationship between GFRP bar and SFRSCC does not have visible impact, but above this deflection level the load carrying capacity is less compared to the model in which perfect bond is assumed. The effect was more pronounced when the higher number of GFRP bars applied.
- The tensile stress of GFRP bar corresponding to crack width limit state of 0.3 mm was lower in case of allowing sliding between GFRP and surrounding SFRSCC than assuming perfect bond. That means, when sliding in GFRP bar was allowed, the lower tensile stress was attained in GFRP bar. This can be improved with increasing the number of bars.

ACKNOWLEDGEMENTS

The authors acknowledge support provided by FCT - Fundação para a Ciência e a Tecnologia. The study presented in this paper is a part of the research project titled “DURCOST - Innovation in reinforcing systems for sustainable pre-fabricated structures of higher durability and enhanced structural performance” with reference number of PTDC/ECM/105700/2008. The authors also thank the collaboration of the following companies: Schock for providing the GFRP bars, Casais to manufacture the moulds, Maccaferri for supplying the steel fibers, Secil/Unibetão for providing the Cement, SIKA for providing the superplasticizers; CiviTest for the production of SFRSCC specimens**.**

REFERENCES

[1] Harris HG, Somboonsong W. and Ko FK. “New ductile hybrid FRP reinforcing bar for concrete structures”, ASCE J Compos Constr, 2(1), 28–37 (1998).
[2] Denvid Lau and Hoat Joen Pam, “Experimental study of hybrid FRP reinforced concrete beams”, Engineering Structures, 32, 3857–3865 (2010).
[3] Alsayed, S. H. _1998_. “Flexural behaviour of concrete beams reinforced with GFRP bars.” Cem. Concr. Compos., 20, 1–11.
[4] Wenjun Qu, Xiaoliang Zhang, and Haiqun Huang, “Flexural Behavior of Concrete Beams Reinforced with Hybrid GFRP and Steel Bars”, Journal of Composites for Construction, Vol. 13, No. 5, October 1, 2009.
[5] Li VC, Wang S. “Flexural behaviors of glass fiber-reinforced polymer (GFRP) reinforced engineered cementitious composite beams.”, ACI Mater J 2002;99(1):11–21.
[6] Maria Antonietta Aiello; Marianovella Leone; and Marisa Pecce. Bond Performances of FRP Rebars-Reinforced Concrete. J. Mater. Civ. Eng. 2007; 19(3) 205-213.
[7] Zenon Achillides and Kypros Pilakoutas. Bond Behavior of Fiber Reinforced Polymer Bars under Direct Pullout Conditions. J. Compos Constr 2004; 8(2) 173-181.
[8] Almusallam TH. Analytical prediction of flexural behavior of concrete beams reinforced by fiber reinforced polymer (FRP) bars. J Compos Mater 1997; 31(7):640–57.
[9] Masmoudi R, Theriault M, Benmokrane B. Flexural behavior of concrete beams reinforced with deformed fiber reinforced plastic reinforcing rods. ACI Struct J 1998;95(6):665–76.
[10] H.A. Abdalla. Evaluation of deflection in concrete members reinforced with fiber reinforced polymer (FRP) bars. Composite Structures 2002; 56 63–71.
[11] Pecce M, Manfredi G, Cosenza E. Experimental response and code models of GFRP RC beams in bending. J Compos Constr 2000; 4(4):182–90.
[12] V. Alunno Rossetti. Local bond stress-slip relationships of glass fiber reinforced plastic bars embedded in concrete. Materials and Structures, 1995, 28, 340-344.
[13] B. Tighiouart, B. BenmokraneU, D. Gao. Investigation of bond in concrete member with fiber reinforced polymer (FRP) bars. Construction and Building Materials 1998; 12 453-462.
[14] Pecce, M., Manfredi, G., Realfonzo, R., and Cosenza, E. “Experimental and analytical evaluation of bond properties of GFRP bars.” J. Mater. Civ. Eng., 2001; 13(4), 282–290.
[15] Roman Okelo, A.M.ASCE, and Robert L. Yuan, P.E., M.ASCE. Bond Strength of Fiber Reinforced Polymer Rebarsin Normal Strength Concrete. J. Compos for Constr 2005; 9(3) 203-213.
[16] Maria Antonietta Aiello; Marianovella Leone; and Marisa Pecce. Bond Performances of FRP Rebars-Reinforced Concrete. J. Mater. Civ. Eng. 2007; 19 (3) 205-213.
[17] Marta Baena, Lluís Torres, Albert Turon, Cristina Barris. Experimental study of bond behavior between concrete and FRP bars using a pull-out test. Composites: Part B 2009; 40 784-797.

[18] Firas AL-mahmoud, Arnaud Castel, Raoul Francois, Christian Tourneur. Effect of surface pre-conditioning on bond of carbon fiber reinforced polymer rods to concrete. Cement & Concrete Composites 2007; 29 677–689.
[19] RILEM (1982), “Bond test for reinforcement steel. 1. Beam test.”, TC9-RC
[20] CEB-FIB, “CEB-FIB Model code 2010 – Design code”, Final draft, Lausanne, Switzerland (2010)
[21] P.L. Domone, “A review of the hardened mechanical properties of self-compacting concrete”, Cement & Concrete Composites, 29, 1–12 (2007).
[22] Cunha, V.M.C.F.; Barros, J.A.O.; Sena-Cruz, J.M., “Modelling the influence of age of steel fibre reinforced self – compacting concrete on its compressive behaviour”, RILEM Materials and Structures Journal, 41(3), 465-478, 2008.
[23] RILEM TC 162-TDF: Test and design methods for steel fiber reinforced concrete. Materials and structures 2002, 35, 579-582 (2003).
[24] Barros, J.A.O., Cunha, V.M.C.F., Ribeiro, A.F., Antunes, J.A.B., “Post-Cracking Behaviour of Steel Fibre Reinforced Concrete", RILEM Materials and Structures Journal, 38(275), 47-56, 2005.
[25] Sena-Cruz, J.M.; Barros, J.A.O.; Ribeiro, A.F.; Azevedo, A.F.M.; Camões, A.F.F.L., "Stress-crack opening relationship of enhanced performance concrete", 9th Portuguese Conference on Fracture, ESTSetúbal, Portugal, p. 395-403, 18-20 February 2004.
[26] Barros, J.A.O.; Costa, I. G.; Ventura-Gouveia, A., “CFRP flexural and shear strengthening technique for RC beams: experimental and numerical research”, Advances in Structural Engineering Journal, 14(3), 559-581, 2011.
[27] Sena-Cruz, J.M., “Strengthening of concrete structure with near-surface mounted CFRP laminate strips”, Ph.D. thesis, Civil engineering department of university of Minho (2004).